Inorg. Chem. **2003**, *42*, 5999–6007

Donor Atom Dependent Geometric Isomers in Mononuclear Oxo–Molybdenum(V) Complexes: Implications for Coordinated Endogenous Ligation in Molybdoenzymes

Carl J. Carrano,*[,†,‡] Balwant S. Chohan,[†,#] Brian S. Hammes,[†,§] Brian W. Kail,[||] Victor N. Nemykin,[||] and Partha Basu*[,||]

Department of Chemistry and Biochemistry, Southwest Texas State University, San Marcos, Texas 78666, and Department of Chemistry and Biochemistry, Duquesne University, Pittsburgh, Pennsylvania 15282

Received December 17, 2002

We have previously demonstrated that the complex [(L1O)MoOCl$_2$], where L1OH = (2-hydroxy-3-*tert*-butyl-5-methylphenyl)bis(3,5-dimethylpyrazolyl)methane, exists as both cis and trans isomers (Kail, B.; Nemykin, V. N.; Davie, S. R.; Carrano, C. J.; Hammes, B. S.; Basu, P. *Inorg. Chem.* **2002**, *41*, 1281–1291). Here, the cis isomer is defined as the geometry with the heteroatom in the equatorial position, and the trans isomer is designated as the geometry with the heteroatom positioned trans to the terminal oxo group. The trans isomer represents the thermodynamically more stable geometry as indicated by its spontaneous formation from the cis isomer. In this report, we show that for complexes of [(LO)MoOCl$_2$], where LOH is the sterically less restrictive (2-hydroxyphenyl)-bis(3,5-dimethylpyrazolyl)methane, only the trans isomer could be isolated, while in the corresponding thiolate containing ligand (2-dimethylethanethiol)bis(3,5-dimethylpyrazolyl)methane (L3SH) only the cis isomer could be observed. In addition, we have isolated and structurally characterized the complex [(L1O)MoO(OPh)(Cl)], a rare example of a species possessing both cis and trans phenolates. Using DFT calculations, we have investigated the origins of the differences in stability between the cis and trans isomers in these complexes and suggest that they are related to the trans influence of the oxo-group. Crystal data for [(LO)MoOCl$_2$] (**1**) include that it crystallizes in the triclinic space group $P\bar{1}$with cell dimensions $a = 8.9607$ (12) Å, $b = 10.596$ (4) Å, $c = 13.2998$ (13) Å, $\alpha = 98.03$ (2)°, $\beta = 103.21$ (2)°, $\gamma = 110.05$(2)°, and $Z = 2$. [(L1O)MoO(OPh)Cl]·2CH$_2$Cl$_2$ (**2**·2CH$_2$Cl$_2$) crystallizes in the triclinic space group $P\bar{1}$, with cell dimensions $a = 12.2740$ (5) Å, $b = 13.0403$ (5) Å, $c = 13.6141$ (6) Å, $\alpha = 65.799$ (2)°, $\beta = 64.487$ (2)°, $\gamma = 65.750$ (2)°, and $Z = 2$. [(L3S)Mo(O)Cl$_2$] (**3**) crystallizes in the orthorhombic space group $Pna2_1$, with cell dimensions $a = 13.2213$ (13) Å, $b = 8.817$ (2) Å, $c = 15.649$ (4) Å, and $Z = 4$. The implications of these results on the function of mononuclear molybdoenzymes such as sulfite oxidase, and the DMSO reductase, are discussed.

Introduction

Mononuclear molybdenum containing enzymes have the general function of catalyzing a net oxygen atom transfer (OAT) to or from a physiological acceptor/donor, with the metal cycling between the +6 and +4 oxidation states. They can be conveniently divided into three major groups based on the structure about the metal center, all of which include one or two pyranopterin cofactors.[1] The sulfite oxidase (SO) family contains a dioxo molydenum center coordinated to the dithiolene unit of the pyranopterin along with a cysteinyl sulfur from the protein. The group exemplified by xanthine oxidase contains one pyranopterin bound to a MoO(S)(H$_2$O) unit with no direct protein based ligation. The final group, the DMSO reductase family, is characterized by a monooxo (or sulfido, selenido) molybdenum center with bis dithiolene

* To whom correspondence should be addressed. E-mail: basu@duq.edu (P.B.).
† Southwest Texas State University.
‡ Current Address: Department of Chemistry, San Diego State University, San Diego, CA 92182.
§ Current Address: Department of Chemistry, St. Joseph's University, Philadelphia, PA 19131.
|| Duquesne University.
Current address: Department of Chemistry, Susquehanna University, Selinsgrove, PA 17810.

(1) Hille, R. *Chem. Rev.* **1996**, *96*, 2757.

10.1021/ic0262785 CCC: $25.00
Published on Web 08/28/2003

coordination from two pterins and a coordination from an endogenous ligand such as a serinato oxygen, or a cysteinato sulfur. However, no such coordination was found in arsenite oxidase, which is also a member of the DMSO reductases family. Boyington et al. have suggested that the coordination of the different amino acids controls the substrate specificity among the members of the DMSO reductase family.[2] Crystal structures for enzymes representing all three families have been determined.[3−5] Interestingly, the diversity in the coordination features of the prokaryotic enzymes are represented by nitrate reductases.[6]

Analogue chemistry has played an invaluable role in understanding the structure and mechanism of metalloproteins including mononuclear molybdoenzymes.[7−11] For example, the detailed and elegant work using the symmetric tris(pyrazolyl)borate Tp^R ligands, as a platform, has resulted in oxo−molybdenum(V) systems that provided valuable insight to spectroscopic signature of the enzymes.[12] Indeed, this early work has given us one of the first forays into the reactivity and spectroscopy of isostructural $[(Tp^R)MoOX_2]$ derivatives (X = OPh^-, OMe^-, and SPh^-). We envisaged polyfunctional, facially coordinating tridentate ligands containing two pyrazole groups with two nitrogen donors, and another donor atom such as the thiolato sulfur or phenolato oxygen would provide an asymmetric donor set. The heteroscorpionate ligand, $(pz)_2CHX$, would produce coordination environments similar to that offered by $(Tp^R)^-$ with the same topology and charge, differing in only one donor atom. Therefore, through the comparison of $(pz)_2CHX$ tripodal ligands, where X contains O or S containing donors, with the well studied $(Tp^R)^-$ will allow a direct understanding of the influence of structure on the reactivity of Mo(V)−oxo complexes. In this report, we describe Mo(V)−oxo complexes with three heteroscorpionate ligands (LO), $(L1O)^-$ and $(L3S)^-$ and their properties (Scheme 1). The results are presented in light of the known geometric preference of the active sites of the mononuclear molybdenum enzymes.

Scheme 1

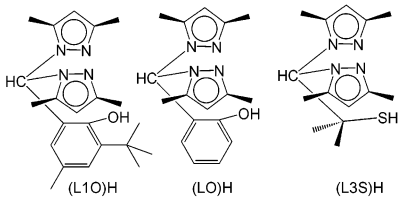

Experimental Section

All syntheses were carried out under an inert atmosphere, while the reagents and solvents were purchased from commercial sources and used as received unless otherwise noted. Once the synthesis was complete, all subsequent workup was carried out in air. Toluene and THF were distilled under argon and dried over Na/benzophenone. The silica gel 60−200 mesh used for the adsorption chromatography and the Celite used for filtration were purchased from the Aldrich Chemical Co. The purity of the isolated compounds, as well as the progress of the reactions, was monitored by thin-layer chromatography. The ligands (2-hydroxyphenyl)bis(3,5-dimethylpyrazolyl)methane (LOH), (3-*tert*-butyl-2-hydroxy-5-methylphenyl)bis(3,5-dimethylpyrazolyl)methane (L1OH), and (2-dimethylethanethiol)bis(3,5-dimethylpyrazolyl)methane (L3SH) were prepared using the previously reported procedures.[13] The complex $[(L1O)MoOCl_2]$ was prepared as described in the literature.[14,15]

$[(LO)MoOCl_2]$ (1). To 40 mL of THF in a 100 mL round-bottom flask was slowly added 2.0 g (7.3 mmol) of $MoCl_5$, and the mixture stirred for 0.5 h. In a separate 100 mL flask, a solution of LOH (2.17 g, 7.3 mmol) in 20 mL of THF was treated with solid KH (0.29 g, 7.3 mmol) and stirred for 0.5 h. The K(L1O) solution was then added dropwise to the green $MoOCl_3(THF)_2$. The resulting solution was stirred for 12 h and filtered to give a red/brown precipitate. The solid was redissolved in CH_2Cl_2 and filtered through Celite to remove a small amount of KCl. The organics were removed under reduced pressure to give 70% yield (2.6 g, 5.1 mmol) of $[(LO)MoOCl_2]$ as a red/brown solid. X-ray quality crystals of $[(LO)MoOCl_2]$ were obtained from hot CH_2Cl_2/hexane as dark red/brown blocks. Anal. Calcd (Found) for $[(LO)Mo(O)Cl_2]$, $C_{17}H_{20}N_4O_2Cl_2Mo$: C, 42.47 (42.61); H, 3.77 (4.21); N, 11.60 (11.69). FTIR (KBr, cm^{-1}): ν_{MoO} = 944(s). λ_{max} (CH_2Cl_2, ϵ, M^{-1} cm^{-1}): 290 (7585), 345 (6800), 424 (sh).

$[(L1O)MoO(OPh)Cl]$ (2). To a slurry of 0.31 g (0.57 mmol) of $[(L1O)MoOCl_2]$ in 30 mL of toluene were added 0.11 g of

(2) Boyington, J. C.; Gladyshev, V. N.; Khangulov, S. V.; Stadtman, T. C.; Sun, P. D. *Science* **1997**, *275*, 1305−1308.
(3) Huber, R.; Hof, P.; Duarte, R. O.; Moura, I.; Liu, M.; LeGall, J.; Hille, R.; Archer, M.; Romao, M. J. *Proc. Natl. Acad. Sci. U.S.A.* **1996**, *93*, 8846.
(4) Schindelin, H.; Kisker, C.; Rees, D. C. *JBIC, J. Biol. Inorg. Chem.* **1997**, *2*, 773.
(5) Kisker, C.; Schindelin, H.; Pacheco, A.; Wehbi, W. A.; Garrett, R. M.; Rajagopalan, K. V.; Enemark, J. H.; Rees, D. C. *Cell* **1997**, *91*, 973.
(6) Stolz, J. F.; Basu, P. *ChemBioChem*. **2002**, *3*, 198−206.
(7) (a) Musgrave, K. B.; Lim, B. S.; Sung, K.-M.; Holm, R. H.; Hedman, B.; Hodgson, K. O. *Inorg. Chem*. **2000**, *39*, 5238−5247. (b) Lim, B. S.; Sung, K.-M.; Holm, R. H. *J. Am. Chem. Soc.* **2000**, *122*, 7410−7411. (c) Lim, B. S.; Donahue, J. P.; Holm, R. H. *Inorg. Chem*. **2000**, *39*, 263−273. (d) Musgrave, K. B.; Donahue, J. P.; Lorber, C.; Holm, R. H.; Hedman, B.; Hodgson, K. O. *J. Am. Chem. Soc.* **1999**, *121*, 10297−10307. (e) Sung, K.-M.; Holm, R. H. *J. Am. Chem. Soc.* **2001**, *123*, 1931−1943. Lim, B. S.; Holm, R. H. *J. Am. Chem. Soc.* **2001**, *123*, 1920−1930. (f) Donahue, J. P.; Goldsmith, C. R.; Nadiminti, U.; Holm, R. H. *J. Am. Chem. Soc.* **1998**, *120*, 12869−12881. (g) Donahue, J. P.; Lorber, C.; Nordlander, E.; Holm, R. H. *J. Am. Chem. Soc.* **1998**, *120*, 3259−3260.
(8) Xiao, Z.; Young, C. G.; Enemark, J. H.; Wedd, A. G. *J. Am. Chem. Soc.* **1992**, *114*, 9194−9195. Laughlin, L. J.; Young, C. Y. *Inorg. Chem.* **1996**, *35*, 1050−1058.
(9) Das, S. K.; Choudhury, P. K.; Biswas, D.; Sarker, S. *J. Am. Chem. Soc.* **1994**, *116*, 9061−9070. Oku, H.; Ueyama, N.; Kondo, M.; Nakamura, A. *Inorg. Chem.* **1994**, *33*, 209−216. Ueyama, N.; Okamura, T.; Nakamura, A. *J. Am. Chem. Soc.* **1992**, *114*, 8129−8137.
(10) (a) Smith, P. D.; Millar, A. J.; Young, C. G.; Ghosh, A.; Basu, P. *J. Am. Chem. Soc.* **2000**, *122*, 9298−9299. (b) Mondal, S.; Basu, P. *Inorg. Chem*. **2001**, *40*, 192−193. (c) Nemykin, V. N.; Davie, S. R.; Mondal, S.; Rubie, N.; Somogyi, A.; Kirk, M. L.; Basu, P. *J. Am. Chem. Soc.* **2002**, *124*, 756−757.
(11) Inscore, F. E.; McNaughton, R.; Westcott, B. L.; Helton, M. E.; Jones, R.; Dhawan, I. K.; Enemark, J. H.; Kirk, M. L. *Inorg. Chem.* **1999**, *38*, 1401−1410. McNaughton, R. L.; Helton, M. E.; Rubie, N. D.; Kirk, M. L. *Inorg. Chem.* **2000**, *39*, 4386−4387.
(12) (a) Cleland, W. E.; Barnhart, K. M.; Yamanouchi, K.; Collison, D.; Mabbs, F. E.; Ortega, R. B.; Enemark, J. H. *Inorg. Chem.* **1987**, *26*, 1017−1025. (b) Roberts. S. A.; Young, C. G.; Kipke, C. A.; Cleland, W. E.; Yamanouchi, K.; Carducci, M. D.; Enemark, J. H. *Inorg. Chem.* **1990**, *29*, 3650. (c) Dhawan, I. K.; Pacheco, A.; Enemark, J. H. *J. Am. Chem. Soc.* **1994**, *116*, 7911.
(13) Hammes, B. S.; Carrano, C. J. *Inorg. Chem.* **1999**, *38*, 666. Hammes, B. S.; Carrano, C. J. *J. Chem. Soc., Dalton Trans* **2000**, 3304−3309.
(14) Davie, S. R.; Rubie, N.; Hammes, B. S.; Carrano, C. J.; Kirk, M. L.; Basu, P. *Inorg. Chem.* **2001**, *40*, 2632−2633.
(15) Kail, B.; Nemykin, V. N.; Davie, S. R.; Carrano, C. J.; Hammes, B. S.; Basu, P. *Inorg. Chem*. **2002**, *41*, 1281−1291.

triethylamine and 0.11 g (1.1 mmol) of HOPh. The reaction was warmed to 75 °C and stirred for 24 h, after which the reaction mixture was filtered to remove a dark red precipitate. The red precipitate was dissolved in CH_2Cl_2, filtered to remove any Et_3N·HCl, and dried under reduced pressure to give 0.26 g (0.39 mmol; 68% yield based on **1**) of [(L1O)Mo(O)(OPh)(Cl)] as a dark red solid. X-ray quality crystals of [(L1O)Mo(O)(OPh)(Cl)] were isolated by slow evaporation of a 2:1 CH_2Cl_2/pentane solution containing [(L1O)Mo(O)(OPh)(Cl)] (**2**). Anal. Calcd (Found) for [(L1O)MoO(OPh)Cl], $C_{28}H_{34}N_4O_3ClMo$: C, 55.49 (55.30); H, 5.67 (5.75); N, 9.24 (9.11). FTIR (KBr, cm^{-1}): ν_{MoO} = 942 (s). λ_{max} (CH_2Cl_2, ϵ, M^{-1} cm^{-1}): 300 (7600), 338 (6400), 502 (1300). μ_{eff} = 1.93 μ_{BM} (solid, 296 K).

[(L3S)MoOCl$_2$] (3). To 30 mL of THF in a 100 mL round-bottom flask was slowly added 0.51 g (1.9 mmol) of $MoCl_5$, and the mixture stirred for 0.5 h. In a separate 100 mL flask, a solution of L3SH (0.52 g, 1.9 mmol) in 15 mL of THF was treated with solid KH (0.075 g, 1.9 mmol) and stirred for 0.5 h. The K(L3S) solution was then added dropwise to the green $MoOCl_3(THF)_2$ reactant. The resulting solution was stirred for 12 h and filtered to give a green precipitate. The solid was dissolved in CH_2Cl_2 and filtered through Celite to remove a small amount of KCl. The organic solvents were removed under reduced pressure to give [(L3S)Mo(O)Cl_2] as a green solid. Crystallization was accomplished by layering a concentrated CH_2Cl_2 solution of **3** with isopropyl ether to yield 0.35 g (0.78 mmol; yield 41%) of the complex. Anal. Calcd (Found) for [(L3S)MoOCl_2], $C_{14}H_{21}N_4OSCl_2Mo$: C, 36.53 (36.51); H, 4.61 (4.60); N, 12.17 (12.06). FTIR (KBr, cm^{-1}): ν_{MoO} = 957 (s). λ_{max} (CH_2Cl_2, ϵ, $M^{-1}cm^{-1}$): 346 (3550), 434 (1140), 628 (484). μ_{eff} = 1.86 μ_{BM} (solid, 296 K).

Physical Methods. Elemental analyses were performed on all compounds by Quantitative Technologies, Inc., Whitehouse, NJ. All samples were dried in a vacuum prior to analysis. IR spectra were recorded from KBr disks on a Perkin-Elmer 1600 series FTIR spectrometer and are reported in wavenumbers. Cyclic voltammetric experiments were conducted using a BAS CV 50W (Bioanalytical Systems Inc., West Lafayette, IN) voltammetric analyzer. All experiments were done under argon at ambient temperature in solutions with 0.1 M tetrabutylammonium hexafluorophosphate as the supporting electrolyte. Cyclic voltammograms (CVs) were obtained using a three-electrode system consisting of glassy-carbon working, platinum wire auxiliary, and saturated calomel electrode (SCE) reference electrodes. The ferrocenium/ferrocene couple was used to monitor the reference electrode and was observed at 0.468 V with ΔE_p = 0.120 V and $i_{pc}/i_{pa} \cong 1.0$ in CH_2Cl_2. Internal resistance compensation was applied before each CV was recorded. Potentials are reported versus the saturated calomel couple. Electronic spectra were recorded using a Varian Cary 50 spectrophotometer. Room temperature magnetic susceptibility measurements of the metal complexes were determined using a magnetic susceptibility balance MSB-1 manufactured by Johnson Matthey and calibrated with mercury(II) tetrathiocyanatocobaltate(II) (χ_g = 16.44(8) × 10^{-6} cm^3 g^{-1}).[16] Diamagnetic corrections were taken from those reported by O'Connor.[17]

Crystallographic Details. The crystal data collection and refinement parameters for [(LO)MoOCl_2] (**1**), [(L1O)MoO(OPh)-Cl] (**2**), and [(L3S)MoOCl_2] (**3**) are given in Table 1. Crystals of all complexes were sealed in thin-walled quartz capillaries prior to the data collection at 298 K for **1** and at 153 and 198 K for **2** and **3**, respectively. All crystals, except those of **2**, were mounted on a Siemens P4 diffractometer with a sealed-tube Mo X-ray source and controlled via personal computer running Siemens XSCANS 2.1. Crystals of [(L1O)MoO(OPh)Cl] were collected on a Nonius Kappa CCD diffractometer using a graphite monochromator. The systematic absences in the diffraction data are consistent with the space groups $P\bar{1}$ for [(LO)MoOCl_2], $P\bar{1}$ for [(L1O)Mo(O)(OPh)Cl]·$2CH_2Cl_2$, and $Pna2_1$ for [(L3S)Mo(O)Cl_2]. The structures were solved using direct methods or via the Patterson function, completed by subsequent difference Fourier syntheses, and refined by full-matrix least-squares procedures on F^2. The asymmetric unit of [(LO)MoOCl_2]·CH_2Cl_2 contains one fully occupied and relatively ordered dichloromethane molecule of solvation. The asymmetric unit of [(L1O)MoO(OPh)Cl]·$2CH_2Cl_2$ contains one well ordered molecule of CH_2Cl_2 and a partially disordered one. The disordered solvent was modeled with one fully occupied Cl atom, and a second that was disordered over 2-positions, each with occupancies of 0.5.

All non-hydrogen atoms were refined with anisotropic displacement coefficients and treated as idealized contributions using a riding model, except where noted. Software and sources of the scattering factors are contained in the SHELXTL (5.0) program library (G. Sheldrick, Siemens XRD, Madison WI).

Computational Details. All density functional calculations were performed on the intact complexes using Becke's three-parameter hybrid exchange functional[18] and the Lee−Yang−Parr nonlocal correlation functional[19] (B3LYP) within the borders of unrestricted

Table 1. Summary of Crystallographic Data and Parameters for [(LO)MoOCl_2] (**1**), [(L1O)MoO(OPh)Cl] (**2**), and [(L3S)MoOCl_2] (**3**)

	1·CH_2Cl_2	**2**·$2CH_2Cl_2$	**3**
molecular formula	$C_{18}H_{21}N_4Cl_4MoO_2$	$C_{30}H_{38}Cl_5N_4O_3Mo$	$C_{14}H_{21}N_4OCl_2SMo$
fw	563.13	775.93	460.29
temp (K)	293(2)	153(2)	198(2)
cryst syst	rhombohedral	triclinic	orthorhombic
space group	$P\bar{1}$	$P\bar{1}$	$Pna2_1$
cell constants			
a (Å)	8.9607(12)	12.2740(5)	13.2213(13)
b (Å)	10.596(4)	13.0403(5)	8.814(2)
c (Å)	13.2998(13)	13.6141(6)	15.649(4)
α (deg)	98.03(2)	65.799(2)	90
β (deg)	103.21(2)	64.487(2)	90
γ (deg)	110.05(2)	65.750(2)	90
Z	2	2	4
V (Å^3)	1121.6(5)	1719.61(12)	1823.6(6)
abs coeff, μ_{calcd} (mm^{-1})	1.083	0.728	1.079
δ_{calcd} (g/cm^3)	1.667	1.449	1.685
F(000)	566	780	936
cryst dimens (mm^3)	0.1 × 0.4 × 0.6	0.2 × 0.4 × 0.05	0.9 × 0.8 × 0.7
radiation	Mo Kα (λ = 0.71073 Å)	Mo Kα (λ = 0.71073 Å)	Mo Kα (λ = 0.71073 Å)
h,k,l ranges collected	0 → 9 −11 → 10 −14 → 13	−5 → 5 −17 → 18 −18 → 18	−14 → 0 0 → −9 −14 → 0
θ range (deg)	2.11−22.50	2.96−30.10	2.60−22.50
no. reflns collected	3095	11239	1084
no. unique reflns	2873	4232	1084
no. params	262	393	208
data/param ratio	10.96	10.77	5.20
refinement method	full-matrix least-squares on F^2	full-matrix least-squares on F^2	full-matrix least-squares on F^2
$R(F)^a$	0.0963	0.0650	0.0505
$R_w(F^2)^b$	0.2090	0.1863	0.1314
$GOF_w{}^c$	1.008	1.059	0.979
largest diff peak and hole (e/Å^3)	1.153 and − 1.356	1.039 and −1.256	0.440 and −0.744

^{a} $R = [\sum|\Delta F|/\sum|F_o|]$. ^{b} $R_w = [\sum w(\Delta F)^2/\sum wF_o^2]$. ^{c} Goodness of fit on F^2.

(16) Figgis, B. N.; Nyholm, J. *J. Chem. Soc.* **1958**, 4190.
(17) O'Connor, C. J. *Prog. Inorg. Chem.* **1992**, *29*, 203.
(18) Becke, A. D. *J. Chem. Phys.* **1993**, *98*, 5648.

and restricted-open Hartree−Hock formalism, without symmetry restrictions. Optimized geometries were obtained by using the B3LYP exchange-correlation functional with a 3-21G* basis set for all atoms under the unrestricted formalism. In the single-point DFT calculations, the molybdenum atom is described with a DGauss full electron double-ζ basis set, with polarization having a (18s,12p,9d) → [6s,5p,3d] contraction scheme;[20] for all other atoms, the standard 6-311G(d) basis set[21] was used. All single point and geometry optimized DFT calculations were performed using the Gaussian 98 program family running under a Windows or a Linux operating system.[22] The percent contribution from the atomic orbitals, to their respective molecular orbitals, was calculated using the VMOdes program.[23]

Results

Synthesis and Reactivity. The treatment of 1 equiv of the deprotonated ligand $(LO)^-$ or $(L3S)^-$ with a THF solution of $MoOCl_3(THF)_2$, as described,[24] affords the red [(LO)$MoOCl_2$] and the green [(L3S)$MoOCl_2$] complex, respectively. For [(LO)$MoOCl_2$], crystallization from dichloromethane produced X-ray quality crystals, structural analysis of which demonstrates only the trans geometry. The trans isomer of [(LO)$MoOCl_2$] is less stable in air and water than the corresponding [(L1O)$MoOCl_2$] complex and decomposes to a blue compound. The composition of this material is presently unknown; however, it may be a polynuclear complex.

Substitution of one chloride ligand can be accomplished by treating a toluene slurry of [(L1O)$MoOCl_2$] with excess phenol (HOPh) at elevated temperatures. Only the monosubstituted complex [(L1O)Mo(O)(OPh)Cl] was isolated, after even 7 days at 80 °C. Treatment of [(L1O)$MoOCl_2$] with a variety of other exogenous ligands failed to facilitate substitution of either or both of the chloride ligands.

For [(L3S)$MoOCl_2$], slow diffusion of hexane into a concentrated solution of CH_2Cl_2 produces green crystals. Typical yields are between 60% and 70%. In stark contrast to [(LO)$MoOCl_2$] or [(L1O)$MoOCl_2$], where the trans isomer has been both computationally and experimentally shown to be the more stable (vide infra). The X-ray crystallographic analysis of the green crystals of [(L3S)$MoOCl_2$] reveals the presence only of the cis isomer that is both air and water stable. However, unlike [(L1O)$MoOCl_2$], substitution reactions at elevated temperatures and extended reaction times (several days) between [(L3S)$MoOCl_2$] and a variety exogenous ligands proved unsuccessful.

Solid-State Structure of the Complexes. The single-crystal X-ray diffraction studies on [(LO)$MoOCl_2$] (**1**), [(L1O)MoO(OPh)Cl] (**2**), and [(L3S)$MoOCl_2$] (**3**) confirm that the $(LO)^-$, $(L1O)^-$, and $(L3S)^-$, formed by deprotonation of the phenol oxygen or alkanethiol sulfur, respectively, bind to molybdenum in a tridentate fashion. Selected bond distances and angles for these complexes are shown in Tables 2 and 3, while Figures 1−3 contain the thermal ellipsoid diagrams of the complexes. Additional structural parameters are provided in the Supporting Information.

Table 2. Selected Bond Distances (Å) for [(LO)$MoOCl_2$] (**1**), [(L1O)MoO(OPh)Cl] (**2**), and [(L3S)$MoOCl_2$] (**3**)[a]

	1	2	3
Mo(1)−N(1)	2.16(2)	2.211(6)	2.36(2)
Mo(1)−N(3)	2.21(2)	2.187(4)	2.24(2)
Mo(1)−S(1)			2.355(3)
Mo(1)−O(1)	1.663(12)	1.690(6)	1.980(9)[b]
Mo(1)−O(2)	1.962(12)	1.976(6)	
Mo(1)−O(3)		1.974(5)	
Mo(1)−Cl(1)	2.378(6)	2.3722(14)	2.380(3)
Mo(1)−Cl(2)	2.351(6)		2.066(10)[b]

[a] Numbers in parentheses are estimated standard deviations. [b] O(1) and Cl(2) are disordered

Table 3. Selected Bond Angles (deg) for [(LO)$MoOCl_2$] (**1**), [(L1O)MoO(OPh)Cl] (**2**), and [(L3S)$MoOCl_2$] (**3**)[a]

	1	2	3
N(1)−Mo(1)−N(3)	81.4(6)	82.0(2)	77.9(3)
N(1)−Mo(1)−S(1)			83.9(4)
N(1)−Mo(1)−O(1)	89.1(6)	87.5(3)	89.3(6)
N(1)−Mo(1)−O(2)	83.2(6)	82.2(2)	
N(1)−Mo(1)−Cl(1)	171.5(5)	93.91(12)	83.2(4)
N(1)−Mo(1)−Cl(2)	92.8(4)		178.6(5)
N(1)−Mo(1)−O(3)		169.1(2)	
N(3)−Mo(1)−O(1)	88.8(6)	87.5(2)	167.1(6)
N(3)−Mo(1)−O(2)	82.1(6)	82.5(2)	
N(3)−Mo(1)−O(3)		90.8(2)	
N(3)−Mo(1)−S(1)			84.9(4)
N(3)−Mo(1)−Cl(1)	93.0(5)	171.9(2)	84.6(4)
N(3)−Mo(1)−Cl(2)	171.2(5)		101.9(5)
O(1)−Mo(1)−O(2)	168.8(7)	166.5(2)	
O(1)−Mo(1)−Cl(1)	97.4(5)	99.4(2)	94.8(4)
O(1)−Mo(1)−Cl(2)	97.7(5)		91.9(4)
O(1)−Mo(1)−O(3)		100.5(3)	
O(1)−Mo(1)−S(1)			93.0(4)
O(2)−Mo(1)−O(3)		88.8(2)	
O(2)−Mo(1)−Cl(1)	89.6(4)	90.00(12)	
O(2)−Mo(1)−S(1)			
O(3)−Mo(1)−Cl(1)		92.16(13)	
S(1)−Mo(1)−Cl(1)			164.84(11)
S(1)−Mo(1)−Cl(2)			94.7(4)
Cl(1)−Mo(1)−Cl(2)	91.9(2)		98.1(3)

[a] Numbers in parentheses are estimated standard deviations.

(19) Lee, C.; Yang, W.; Parr, R. G. *Phys. Rev. B* **1988**, *37*, 785.
(20) Basis sets were obtained from the Extensible Computational Chemistry Environment Basis Set Database, Version 4/22/01, as developed and distributed by the Molecular Science Computing Facility, Environmental and Molecular Sciences Laboratory which is part of the Pacific Northwest Laboratory, P.O. Box 999, Richland, WA 99352, USA, and funded by the U.S. Department of Energy. The Pacific Northwest Laboratory is a multiprogram laboratory operated by Battelle Memorial Institute for the U.S. Department of Energy under Contract DE-AC06-76RLO 1830. Contact David Feller or Karen Schuchardt for further information.
(21) McLean, A. D.; Chandler, G. S. *J. Chem. Phys.* **1980**, *72*, 5639. Krishnan, R.; Binkley, J. S.; Seeger, R.; Pople, J. A. *J. Chem. Phys.* **1980**, *72*, 650.
(22) Frisch, M. J.; Trucks, G. W.; Schlegel, H. B.; Scuseria, G. E.; Robb, M. A.; Cheeseman, J. R.; Zakrzewski, V. G.; Montgomery, J. A., Jr.; Stratmann, R. E.; Burant, J. C.; Dapprich, S.; Millam, J. M.; Daniels, A. D.; Kudin, K. N.; Strain, M. C.; Farkas, O.; Tomasi, J.; Barone, V.; Cossi, M.; Cammi, R.; Mennucci, B.; Pomelli, C.; Adamo, C.; Clifford, S.; Ochterski, J.; Petersson, G. A.; Ayala, P. Y.; Cui, Q.; Morokuma, K.; Malick, D. K.; Rabuck, A. D.; Raghavachari, K.; Foresman, J. B.; Cioslowski, J.; Ortiz, J. V.; Stefanov, B. B.; Liu, G.; Liashenko, A.; Piskorz, P.; Komaromi, I.; Gomperts, R.; Martin, R. L.; Fox, D. J.; Keith, T.; Al-Laham, M. A.; Peng, C. Y.; Nanayakkara, A.; Gonzalez, C.; Challacombe, M.; Gill, P. M. W.; Johnson, B. G.; Chen, W.; Wong, M. W.; Andres, J. L.; Head-Gordon, M.; Replogle, E. S.; Pople, J. A. *Gaussian 98*; Gaussian, Inc.: Pittsburgh, PA, 1998.
(23) Nemykin, V. N.; Basu, P. *VMOdes: Virtual Molecular Orbital description program for Gaussian, GAMESS, and HyperChem*, revision B 6.2.
(24) Cleland. W. E.; Barnhart, K. M. Yamanouchi, K.; Collison, D.; Mabbs, F. E.; Ortega, R. B.; Enemark, J. H. *Inorg. Chem.* **1987**, *26*, 1017.

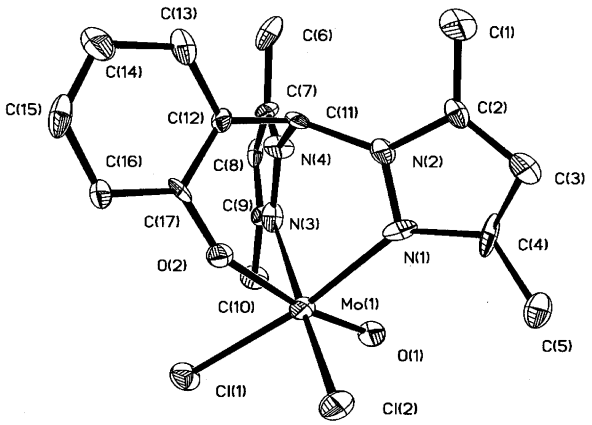

Figure 1. ORTEP plot of **1** at 20% probability ellipsoid.

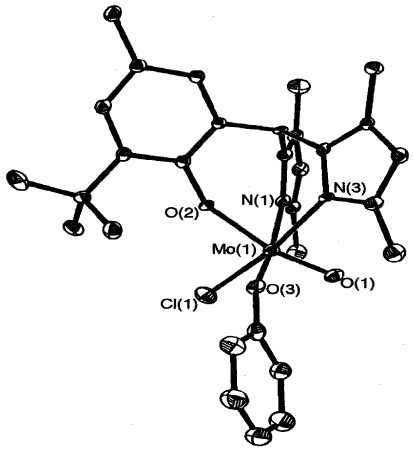

Figure 2. ORTEP plot of **2** at 20% probability ellipsoid.

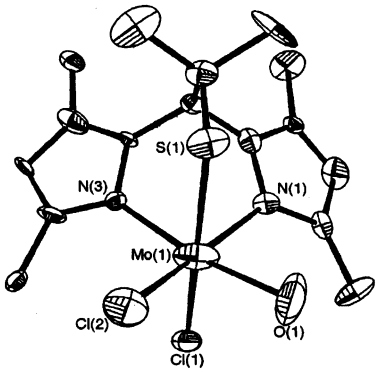

Figure 3. ORTEP plot of **3** at 20% probability ellipsoid.

[(LO)MoOCl$_2$] (1). Unlike [(L1O)MoOCl$_2$], where a compositional disorder between the terminal oxo and the chloro ligands precluded characterization of a single geometric isomer,[15] [(LO)MoOCl$_2$] crystallizes without such disorder and can thus be identified as exclusively the trans isomer. The average N_{pz}−Mo(1)−O(2) bond angle is 84.1(6)°, and the N(1)−Mo(1)−N(3) bond angle is 81.3(8)°. Both the N(1)−Mo(1)−N(3) and average N_{pz}−Mo(1)−O(2) bond angles in the complex deviate from the 90° expected for idealized octahedral geometry due to the relatively small bite angle of the ligand. The seven-membered ring, which contains the phenolate oxygen, supports the larger internal angle. The Mo(1)−O(2) and average Mo−N_{pz} bond distances are 1.96(1) and 2.18(2) Å, respectively. These distances are not unusual and are similar to those reported for other molybdenum complexes.[17]

[(L1O)MoO(OPh)Cl] (2). Figure 2 displays the octahedral coordination geometry around the molybdenum ion with the two pyrazolyl nitrogens and one phenolate oxygen donor from (L1O)$^-$ constituting one face of the octahedron. The N(1)−Mo(1)−N(3) and average N_{pz}−Mo(1)−O(2) bond angles are 82.0(2)° and 82.3(1)°, respectively. The deviation of bond angles from the 90° angle that is expected for idealized octahedral geometry is presumably due to the relatively small bite angle of the ligand. The oxo ligand, O(1), is positioned trans to the phenolate oxygen O(2) with a Mo(1)−O(1) bond distance of 1.690(6) Å, a Mo−O(2) distance of 1.976(4) Å, and a O(1)−Mo(1)−O(2) bond angle of 166.5(2)°. The phenolic oxygen is oriented opposite to one of the pyrazol nitrogen atoms with the O(3)−Mo(1)−N(1) bond angle of 169.0(2)°. The exogenous phenolate ligand is positioned trans to the pyrazolyl nitrogen N(1) with a Mo(1)−O(3) bond distance virtually indistinguishable from the Mo−O(2) distance at 1.974(5) Å. The chloride ligand Cl(1) is trans to the pyrazolyl nitrogen N(3) with a Mo(1)−Cl(1) bond distance of 2.3722(14) Å. The remaining bond distances and angles observed in [(L1O)MoO(OPh)-Cl] are unremarkable and are similar to those reported for other molybdenum(V)−oxo complexes.[24]

[(L3S)MoOCl$_2$] (3). The molecular structure of [(L3S)-MoOCl$_2$] reveals a 2-fold disorder between O(1) and Cl(2). Nevertheless, the solid-state structure clearly shows that the complex must exist exclusively as the cis isomer. The N_{pz}−Mo(1)−S(1) angles for the complex are statistically identical at 83.9(4)° and 84.6(4)°, while the N(1)−Mo(1)−N(3) bond angle is smaller at 77.9(3)°. The thiolate sulfur S(1) lies perpendicular to the square plane formed by the two pyrazolyl nitrogens, one chloride (Cl(2)), and one oxo oxygen. It is trans to the ordered chloride atom Cl(1) with a Mo(1)−S(1) bond distance of 2.355(3) Å and a S(1)−Mo(1)−Cl(1) angle of 164.84(11)°. The Mo(1)−N_{pz} distances observed in [(L3S)MoOCl$_2$] are not unusual and are similar to those reported for other Mo(V)−N_{pz} containing complexes.[19−21] The metal ion lies in the square plane formed by the two pyrazolyl nitrogen atoms, one chlorine (Cl(2)), and one oxo oxygen. The oxo oxygen O(1) is positioned trans to the pyrazolyl nitrogen N(3) with a Mo(1)−O(1) bond distance that is considerably longer than expected (Mo(1)−O(1) = 1.980 Å), the result of the 2-fold disorder between it and the chloride ion Cl(2) which has a bond length shorter than expected (Mo(1)−Cl(2) = 2.066(10) Å). The N(3)−Mo(1)−O(1) angle is 167.1(6)°.

Electrochemistry. The electrochemical behavior of the [(LO)MoOCl$_2$], [(L1O)MoO(OPh)Cl], and [(L3S)MoOCl$_2$] complexes was examined by cyclic voltammetry and Osteryoung square wave voltammetry. The results for the cyclic voltammetric experiments are presented in Table 4.

The cyclic voltammogram of [(L1O)MoO(OPh)Cl], shown in Figure 4, displays two quasireversible redox processes with

Table 4. Electrochemical[a] Properties of [(L1O)$MoOCl_2$], [(L1O)MoO(OPh)Cl], and [(L3S)$MoOCl_2$]

complex	$E_{1/2}$ (V)	ΔE_p (mV)	i_c/i_a
[(LO)$MoOCl_2$]	−0.27	72	0.91
[(L1O)MoO(OPh)Cl]	−0.89, 0.94	92, 156	0.94, 0.99
[(L3S)$MoOCl_2$]	−0.48, 1.30(irr)	77	0.93
cis-(L1O)$MoOCl_2$[b]	−0.70, 1.18	62, 70	
trans-(L1O)$MoOCl_2$[b]	−0.49, 1.31	83, 65	

[a] In CH_2Cl_2 at a scan rate of 0.10 V·s^{-1}; all data are presented with respect to SCE. [b] In MeCN (ref 15).

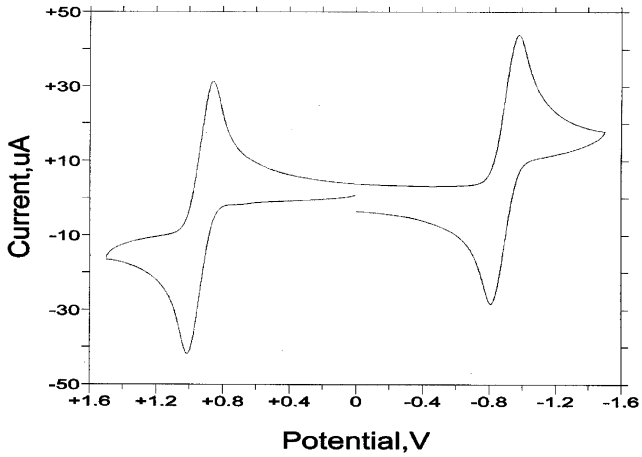

Figure 4. Cyclic voltammogram of **2** in CH_2Cl_2 at 25 °C and scan rate of 100 mV/s.

$E_{1/2} = -0.89$ V for the reductive Mo(IV/V) couple and +0.94 V for the oxidative Mo(V/VI) couple. The potential difference between the two couples of 1.8 V is typical for complexes of this type but is significantly larger than those observed for enzymatic centers. In general, one electron oxidations of Mo(V) complexes are often irreversible due to the inherent instability of mono-oxo Mo(VI) species. This is primarily due to formation of more stable dioxo $[MoO_2]^{2+}$ moieties from traces of water present in the solvent. It is significant that the oxidative wave in **2** is nearly reversible and experiences no substantial decrease in current during repeated scans. This suggests that, at least in the CV time scale, a stable mono-oxo Mo(VI) species is formed due to the presence of the second phenolate group, which mimics the electron donating ability of an oxo group.

The electrochemical response of *cis*-[(L3S)$MoOCl_2$] is similar to that found for **2**. Thus, the CV of *cis*-[(L3S)-$MoOCl_2$] shows a single quasireversible reductive redox process at $E_{1/2} = -0.48$ V with an oxidation process at $E_p = 1.3$ V, again leading to a difference between the couples of about 1.8 V. However, in contrast to **2**, the oxidation process for **3** is largely irreversible and reflects the lower ability of a thiolate donor, in comparison to a phenolate, to stabilize the mono-oxo Mo(VI) moiety.

Cyclic voltammetry of *trans*-[(LO)$MoOCl_2$], in CH_2Cl_2 between 1.5 and −2.0 V versus SCE, shows only one major quasireversible reduction process at $E_{1/2} = -0.27$ V. Thus, it is ∼215 mV more easily reduced than the analogous *tert*-butyl substituted phenolate complex, *trans*-[(L1O)$MoOCl_2$],[15] due to the absence of the electron releasing alkyl groups on the phenol ring. Surprisingly, no reversible oxidation process is observed for **1**. However, given its low reduction potential and the expected difference between oxidative and reductive couples of 1.8 V, the oxidative process is anticipated to appear more positive than +1.5 V, i.e., outside the window of the solvent. A freshly prepared solution of **1** also shows evidence for a small fraction of material (ca. 18%) with a redox potential of −0.48 V. Older solutions contain significantly less of this component. On the basis of our previous results with the [(L1O)$MoOCl_2$] compound, which was isolated in a 2:1 mixture of the cis and trans isomers, we propose that the minor component represents the cis isomer of [(LO)$MoOCl_2$]. The measured ΔE value between the cis and trans isomers of [(LO)$MoOCl_2$] of 210 mV would then be virtually identical to those observed between the cis and the trans isomers of [(L1O)$MoOCl_2$] (213 mV), thus lending strong support for the assignment of the minor component as the cis isomer.

Electronic Structure and Stability Calculations. Because the X-ray crystal structures are not available for *cis*-[(LO)-$MoOCl_2$] or *trans*-[(L3S)$MoOCl_2$], we have used a modern computational approach to understand the influence of the trans effect on the geometry and stability of these complexes. The most important bond distances in the optimized geometries of all of the four possible structures (i.e., cis and trans [(LO)$MoOCl_2$] and [(L3S)$MoOCl_2$]) are presented in Table 5. A comparison of the X-ray determined structures with the optimized geometries shows them to be in good agreement. When the trans effects in both isomers were compared as a function of the heteroatom (i.e., sulfur in L3S and oxygen in LO), the heteroatom in [(L3S)$MoOCl_2$] experiences a 5-fold larger bond elongation than that in [(LO)-$MoOCl_2$]. More explicitly, the Mo−S bond in the [(L3S)-$MoOCl_2$] complex has been calculated to be elongated by nearly 0.1 Å on going from the cis to the trans isomer, while the analogous Mo−O(Ph) bond changes only by 0.02 Å. Experimentally, the X-ray structure of **2** demonstrates that the difference between Mo−O(Ph) bonds cis or trans to an oxo group is even less (essentially zero). Similarly, the Mo−Cl bond distances, in the cis and trans isomers of [(L3S)$MoOCl_2$], differ by 0.06 Å, while that difference is only 0.03 Å for the two isomers of [(LO)$MoOCl_2$]. On the other hand, the Mo═O distances for all four complexes remain essentially invariant. The calculated geometries of the cis and trans isomers of [(L3S)$MoOCl_2$] and [(LO)-$MoOCl_2$] complexes are in good agreement with crystallography. Accordingly, *cis*-[(L3S)$MoOCl_2$] is calculated (using the unrestricted DFT approach) to be 8.7 kcal/mol more stable than the trans isomer, while *trans*-[(LO)$MoOCl_2$] was calculated to be 1.12 kcal/mol more stable than the cis isomer.

The calculated energies of the frontier orbitals for all complexes are shown in Figure 5, and Table 6 lists atomic orbital contribution analysis for selected molecular orbitals. The most important orbital shapes (which are similar in all cases) are depicted in Figure 6. In general the semioccupied orbital has a predominant molybdenum $4d_{xy}$ character and as such is in good agreement with both ligand-field theory and experimental data. In addition, this orbital always

Table 5. Bond Distances from the Optimized Geometries[a]

isomer	Mo=O	Mo−N (trans-O_t)	Mo−N (trans-Cl)	Mo−Cl (trans-N)	Mo−Cl (trans-O/S)	Mo−OPh/ Mo−S(CH)
cis-(LO)$MoOCl_2$	1.70	2.33	2.21	2.37	2.42	1.96
trans-(LO)$MoOCl_2$	1.72 (1.66)	2.26 (2.16)	2.26 (2.21)	2.39 (2.35)	2.39 (2.38)	1.99 (1.96)
cis-(L3S)$MoOCl_2$	1.7 (disordered)	2.42 (2.36)	2.22 (2.24)	2.37 (disordered)	2.43 (2.38)	2.43 (2.36)
trans-(L3S)$MoOCl_2$	1.73	2.25	2.25	2.37	2.37	2.53

[a] Experimental values are in parentheses.

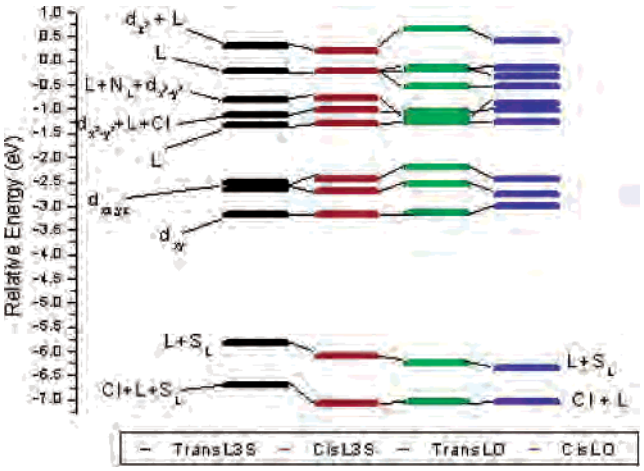

Figure 5. Relative orbital energies for selected molecular orbitals. S_L and O_L represents the heteroatoms of L3S and LO, respectively. The scorpionate ligands are represented by L.

experiences antibonding interactions with the in-plane π-orbitals of the equatorial chlorine atoms. More importantly, the difference in the reduction potential between the cis and trans isomers of [(LO)$MoOCl_2$] (the only complex for which experimental data are available) are in qualitative agreement with the energy difference between their calculated, β-set, LUMO orbitals. Indeed, the energy difference between these orbitals, for the cis and trans isomers of [(LO)$MoOCl_2$], was calculated to be 193 mV, in good agreement with the experimentally observed 207 mV difference. Similarly, the calculated difference in the reduction potential of the cis and trans isomers of [(L3S)$MoOCl_2$] is found to be 66 mV, with the cis isomer being more easily reduced. It should be noted that accurate predictions of the redox potential require a rigorous treatment of the complete redox cycle and the inclusion of solvation effects.[25]

Due to the spin-polarization effect, we have limited the preceding discussion to the spin-unrestricted calculations; however, the electronic structures calculated by the restricted open formalism are discussed in the following text. The calculated LUMO is predominantly molybdenum $4d_{xz}$ in character, and the predicted ordering of the metal orbitals is consistent with ligand field theory for tetragonally distorted octahedral geometry. Accordingly, the next metal-based orbital is the $4d_{yz}$. Interestingly, in all the cases, the molybdenum $4d_{x^2-y^2}$ orbital is delocalized between two molecular orbitals ($d_{x^2-y^2}$ + L and L + $d_{x^2-y^2}$) with the first orbital having a larger metal contribution (Table 6) except in *cis*-[(LO)$MoOCl_2$], where the $d_{x^2-y^2}$ + L orbital is lower in energy than the L + $d_{x^2-y^2}$. Last, the $4d_{z^2}$ orbital has been found to be the highest energy orbital within the d-manifold. Taken together, all of the predominantly molybdenum d-orbitals were found to give the following order of increasing energy: $4d_{xy} < 4d_{xz} \sim 4d_{yz} < 4d_{x^2-y^2} < 4d_{z^2}$.

Another interesting feature revealed by the calculations is that the highest doubly occupied orbital, for all four complexes, had almost purely heteroscorpionate π-orbital character with significant contributions arising from the heteroscorpionate sulfur or oxygen atom. In contrast, the lower energy orbitals are found to be a mixture of the heteroscorpionate ligand and chlorine atom orbitals. Interestingly, the ligand π-acceptor orbitals were found between the molyb-

Table 6. Calculated Orbital Energies and Percent Compositions for [(LO)$MoOCl_2$][a] and [(L3S)$MoOCl_2$][a]

a. [(LO)$MoOCl_2$]

orbital	isomer	energy (eV)	Mo	Mo(d)	O_t	O_L	Cl	N_L	L
Cl + L	cis	−7.048	0.8	0.3	0.3	0.6	81.9	1.7	17.0
	trans	−7.033	1.2	0.4	0.7	0.0	84.6	1.8	13.4
O_L +L	cis	−6.339	4.8	3.3	2.2	23.2	7.4	0.9	85.6
	trans	−6.236	3.8	2.9	2.2	24.4	7.0	1.9	86.9
d_{xy}	cis	−3.013	81.0	80.7	0.1	4.6	9.3	0.4	9.6
	trans	−3.161	81.4	81.3	0.0	0.4	13.4	1.1	5.2
d_{xz}	cis	−2.771	69.8	68.7	14.2	0.1	5.0	2.2	11.0
	trans	−2.533	71.2	70.5	13.0	2.0	2.8	1.1	13.1
d_{yz}	cis	−2.446	71.1	70.1	12.1	3.5	5.8	0.5	11.1
	trans	−2.202	69.7	68.2	13.1	5.1	2.8	0.6	14.3
$d_{x^2-y^2}$ + L	cis	−0.892	48.8	47.7	0.3	4.6	13.5	7.5	37.4
	trans	−1.171	56.4	56.3	0.5	0.0	17.8	11.8	25.2
L + $d_{x^2-y^2}$	cis	−1.028	15.7	15.6	0.2	2.3	4.0	9.0	80.1
	trans	−1.052	12.8	12.8	0.0	0.6	3.6	12.2	83.6
d_{z^2}	cis	0.418	40.3	32.3	6.8	3.3	5.8	7.1	47.1
	trans	0.651	30.1	20.2	4.0	1.4	5.2	2.6	60.7

b. [(L3S)$MoOCl_2$]

orbital	isomer	energy (eV)	Mo	Mo(d)	O_t	S_L	Cl	N_L	L
Cl + L + S_L	cis	−7.071	10.6	5.1	0.5	27.3	47.7	3.0	41.2
	trans	−6.681	14.7	6.3	10.1	49.6	1.8	5.4	73.4
L + S − L + Cl	cis	−6.088	3.2	2.6	4.1	64.6	6.5	3.1	86.2
	trans	−5.831	4.3	3.4	1.5	62.4	10.1	3.2	84.1
d_{xy}	cis	−3.187	81.7	81.4	0.0	2.7	11.8	0.5	6.5
	trans	−3.172	82.4	82.3	0.0	0.6	13.0	1.0	4.6
d_{xz}	cis	−2.700	69.9	68.3	13.7	0.1	5.0	2.5	11.4
	trans	−2.646	71.4	69.9	12.6	4.9	2.9	1.5	13.1
d_{yz}	cis	−2.433	68.0	66.9	12.5	6.0	5.4	0.4	14.1
	trans	−2.520	65.8	62.5	12.6	7.5	5.9	0.8	15.7
$d_{x^2-y^2}$ + L	cis	−1.032	48.8	48.2	0.3	11.7	13.8	6.3	37.1
	trans	−1.123	51.0	50.8	0.3	0.0	16.9	12.3	31.7
L + $d_{x^2-y^2}$	cis	−0.764	8.2	7.8	0.3	1.5	1.8	16.5	89.6
	trans	−0.809	20.8	20.6	0.2	0.1	5.2	17.3	73.8
d_{z^2}	cis	0.201	52.8	36.2	6.8	3.9	5.8	7.9	34.6
	trans	0.311	39.9	30.9	5.8	12.0	4.4	4.7	49.9

[a] Using the restricted open formalism.

(25) Mouesca, J.-M.; Chen, J. L.; Noodleman, L.; Bashford, D.; Case, D. A. *J. Am. Chem. Soc.* **1994**, *116*, 11898−11914.

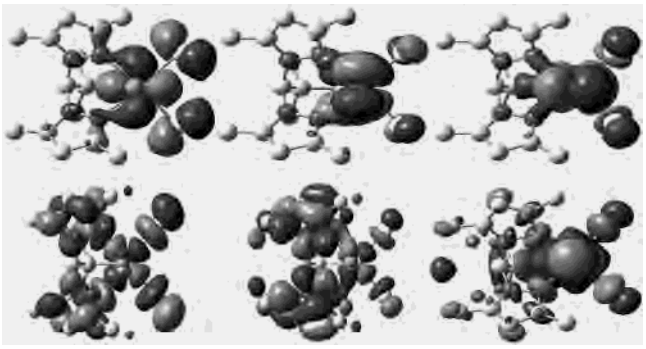

Figure 6. Typical shapes of the frontier d-orbitals in Mo(V) complexes. The orbitals are shown for *trans*-[(L3S)$MoOCl_2$]. From left to right, the molecular orbitals composition are as follows: d_{xy}, d_{xz}, d_{yz}, $d_{x^2-y^2}$ + L, L + $d_{x^2-y^2}$, d_{z^2} (see Table 6).

denum $4d_{yz} - 4d_{x^2-y^2}$ and $4d_{x^2-y^2} - 4d_{z^2}$ orbitals (Table 6), suggesting that low-lying scorpionate π-acceptor orbitals may play a role in defining the electronic structure of these complexes.

Discussion

Both the calculations and the experiments show that, by simply changing the donor atom in an otherwise isoelectronic, isosteric, and isostructural N_2X tripodal ligand system, the relative stability of geometric isomers of [(L)$MoOCl_2$] complexes changes. In the case where $X = O_{phenolate}$, the trans isomer is the more stable while for $X = S_{thiolate}$ it is the cis isomer. One obvious question is concerned with the origin of this effect. The structural trans effect is well-known and widely evoked in oxomolybdenum chemistry. Bond lengths between Mo and atoms trans to the very tightly bound oxo group are usually extensively elongated. For example, the $Mo-N_{trans}$ distances (trans to the oxo group) in [(L3S)MoO(SPh)$_2$], [(L3S)MoO(bdt)], [(Tp*)MoO(SPh)$_2$], and [(Tp*)MoO(bdt)] are 0.2−0.4 Å longer than the corresponding $Mo-N_{cis}$ (cis to the oxo group).[12] Similarly, the calculated $Mo-S_{trans}$ (trans to the oxo group) distance in *trans*-[(L3S)$MoOCl_2$] is 0.1 Å longer that the $Mo-S_{cis}$ (cis to the oxo group) distance in *cis*-[(L3S)$MoOCl_2$]. On the other hand, the expected trans elongation is calculated to be small in *trans*-[(LO)$MoOCl_2$], and crystallographically, no significant trans effect could be observed in [(L1O)MoO(OPh)Cl] (**2**). Interestingly, the latter is a rare example of an oxo−molybdenum complex containing both cis and trans phenolate groups, thus providing an internal reference for evaluating the trans effect induced by the terminal oxo-group. Clearly, in the crystal structure of **2**, both $Mo-O_{phenolate}$ bonds are statistically equivalent (∼1.97 Å) and are similar to the values determined in analogous complexes. Thus, in this complex there is no appreciable trans effect on the $Mo-O_{phenolate}$ bond.

The electrochemical data suggest that geometric reorganization (i.e., isomerization) in these complexes can modulate the molecular redox poise. In the case of [(L3S)$MoOCl_2$], the calculations suggest a difference in the β-LUMO, the redox orbital, of the cis to the trans isomer of ∼66 mV. Although only the cis isomer has been isolated for [(L3S)$MoOCl_2$], it is reasonable to suggest the corresponding trans isomer would be more difficult to reduce, a behavior experimentally verified for [(L1O)$MoOCl_2$] where the cis isomer is ∼213 mV more difficult to reduce than the trans isomer. The reasons for this assumption are 2-fold. First, in all cases, the redox orbital (d_{xy} orbital) has a significantly greater heteroatom character in the cis isomer relative to the trans, while in the trans isomer the redox orbital has a greater chlorine atom character. Second, the energy difference between the d_{xy} orbitals of the cis and trans isomers of [(L3S)$MoOCl_2$] are smaller than those observed in the [(LO)$MoOCl_2$] or [(L1O)$MoOCl_2$] complexes. Thus, it is reasonable to suggest that a geometric change would present smaller differences in redox poise for the complex with the sulfur donor.

A detailed inspection of the DMSOR crystallographic data, and that of a related enzyme trimethylamine *N*-oxide reductase (TMAOR), reveals a wide variation in the reported O_t-Mo-O_{ser} angle (terminal-oxo−Mo−serinato-oxygen), which ranges from 90° to 146°. Recently, an in-depth investigation of the isomeric complexes of the L1O ligand has offered the serine gated electron transfer (SGET) model as a functional implication of this structural variation.[15] A similar comparison for an O(terminal)−Mo−S(cysteine) angle can be made from the crystal structure of chicken liver sulfite oxidase[5] and *Desulfovibrio desulfuricans* nitrate reductase[26] where the O(terminal)−Mo−S(cysteine) angles are 72.8° and 55°, respectively. The magnitudes of the angles are clearly suggestive of a preference for the sulfur donors in the equatorial position as demonstrated with the model complexes. Thus, the model investigation provides an electronic argument of the preferred geometry for the amino acid based donors in DMSO reductase and nitrate reductase.

Finally, when a mismatched coordination is created, via site-directed mutagenesis, the proteins are found to be either less active or inactive as compared to the wild type enzymes. Thus, when cysteine-207 (coordinated to molybdenum) in human sulfite oxidase is mutated to a serine, the enzyme loses its activity, and the extended X-ray absorption fine structure (EXAFS) reveals a trioxo−Mo center at the fully oxidized state.[27,28] In a similar type of experiment, when serine 147 (that coordinates to molybdenum) is mutated to a cysteine in DMSOR, the resultant enzyme is again 61−99% less reactive than the wild-type enzyme.[29] In light of the previously described SGET model, it is provocative to suggest that, in the mutated proteins, a mismatched geometry produced upon coordination of amino acids with different donor groups may be an important controlling factor in the less functional expressed enzymes.

Conclusions

Three new oxo−molybdenum(V) compounds are reported, and all of them are characterized by X-ray crystal-

(26) Dias, J. M.; Than, M. E.; Humm, A.; Huber, R.; Bourenkov, G. P.; Bartunik, H. D.; Bursakov, S.; Calvete, J.; Caldeira, J.; Carneiro, C.; Moura, J. J. G.; Moura, I.; Romão, M. J. *Structure* **1999**, *7*, 65−79.
(27) George, G. N.; Gerrett, R. M.; Prince, R. C.; Rajagopalan, K. V. *J. Am. Chem. Soc.* **1996**, *118*, 8588−8592.
(28) Gerrett, R. M.; Rajagopalan, K. V. *J. Biol. Chem.* **1996**, *271*, 7387−7391.
(29) Hilton, J. C.; Temple, C. A.; Rajagopalan, K. V. *J. Biol. Chem.* **1999**, *274*, 8428−8436.

lography. The geometries of the nonisolated as well as the crystallographically characterized geometric isomers were calculated by DFT methodology. The electronic structures at the metal centers, evaluated by DFT methodology, provide a rationale for the relative reduction potentials and isomeric stability. Using heteroscorpionate ligands, it has been possible to generate a coordination preferred geometric isomer: the phenolic oxygen stabilizes the trans isomer while the thiol coordination stabilizes the cis isomer. In light of the previously reported serine gated electron transfer hypothesis, the mismatched geometry is suggested to be a possible reason for the lack of catalytic efficiency for the genetically engineered sulfite oxidase and DMSO reductases.

Acknowledgment. This work was supported in part by a Scholar-Fellow grant from the Camille and Henry Dreyfus Foundation, the Robert A. Welch Foundation and Grant CHE-9726488 from the NSF to C.J.C. P.B. acknowledges National Institutes of Health (GM 6155501) for financial support of his research program. The NSF-ILI Program Grant USE-9151286 is acknowledged for partial support of the X-ray diffraction facilities at Southwest Texas State University.

Supporting Information Available: Additional crystallographic data and figures (CIF). Additional tables and figures describing computational results. This material is available free of charge via the Internet at http://pubs.acs.org.

IC0262785